Classification
Physics Abstracts
61.12 — 61.25 — 02.70

Bond-orientational order in liquid aluminium$_{80}$-transition metal$_{20}$ alloys

M. Maret ([1]), F. Lançon ([2]) and L. Billard ([2])

([1]) Laboratoire de Thermodynamique et Physico-Chimie Métallurgiques (*), ENSEEG, BP 75, 38402 St-Martin d'Hères Cedex, France
([2]) Département de Recherche Fondamentale sur la Matière Condensée, SP2M/MP, CENG, BP 85X, 38041 Grenoble Cedex, France

(*Received 23 December 1991, revised 18 February 1993, accepted 8 April 1993*)

Abstract. — The structures of liquid $Al_{80}Mn_{20}$ and $Al_{80}Ni_{20}$ are simulated by molecular dynamics using interatomic potentials derived from neutron diffraction data. For these two alloys, the generated three dimensional particle configurations are consistent with the experimental partial pair correlation functions. The characterization of the local symmetries by both the construction of the Voronoï polyhedra and the calculation of the second-order invariants of spherical harmonics allows us to confirm the existence of a local icosahedral order in the quasicrystal-forming liquid $Al_{80}Mn_{20}$ and its absence in liquid $Al_{80}Ni_{20}$ about 70 K above the liquidus line. Molecular dynamics simulations of the corresponding supercooled liquids show that this order increases strongly for $Al_{80}Mn_{20}$ and starts to develop for $Al_{80}Ni_{20}$. An improvement of the agreement between the experimental and calculated pair correlation functions by the reverse Monte Carlo method yields liquid configurations characterized by the same most frequently observed Voronoi polyhedra as those obtained in the molecular dynamics configurations, but with lower percentages.

1. Introduction.

The discovery of quasicrystalline phases in Al-Mn alloys [1] has stimulated the research of local icosahedral order in the corresponding liquid alloys. Such bond-orientational order has already been observed in a supercooled monoatomic liquid by the molecular dynamics method [2] but never above the liquidus line. The neutron scattering experiments performed recently in the aluminium-based liquid alloys — $Al_{80}M_{20}$ [3], $Al_{60}M_{40}$ [4] (M = Mn or the equiatomic mixture Fe-Cr) and $Al_{80}Ni_{20}$ [5] — have yielded a description of the local structure of the liquid in terms of partial pair correlations (i.e. a set of coordination numbers and nearest-neighbour distances). Since the symmetries of the environment around the different species were not accessible from these neutron experiments, no firm conclusion in favour of an icosahedral order could be drawn.

(*) CNRS URA 29.

Nevertheless, from a Landau description of short-range icosahedral order [6] some features in the topological ordering function of the Al-Mn quasicrystal forming liquid alloys (the number-number structure factor $S_{NN}(q)$ in the Bhatia-Thornton formalism [7]) are suggestive of local icosahedral order. These features are the existence of a first peak exceptionally intense for a liquid, the shape of the second peak which tends to form a double-component peak at positions close to 1.7 q_1 and 2 q_1 (q_1 is the first peak position). In contrast, these features are absent in the $S_{NN}(q)$ function of the liquid $Al_{80}Ni_{20}$ which forms no quasicrystal.

The object of this paper is to determine the local symmetries in the two different liquid alloys, $Al_{80}Mn_{20}$ and $Al_{80}Ni_{20}$, from their structure simulated by molecular dynamics using interatomic potentials derived from our previous neutron diffraction data. Information on symmetry is deduced from the 864 atomic positions of the simulated structure : either by dividing into Voronoï polyhedra which can be constructed around each atom or by calculating the bond order parameters introduced in reference [2] which are the second order invariants Q_ℓ formed from the spherical harmonics associated with every bond joining near neighbour atoms. Part of the calculations for $Al_{80}Mn_{20}$ has been briefly presented in reference [8].

In section 2, we present the derivation of the three interatomic pair potentials from neutron data for both liquid alloys, $Al_{80}Mn_{20}$ and $Al_{80}Ni_{20}$. The results of molecular dynamics (MD) performed at 1 320 K (i.e. about 70 K above the melting temperature, T_m) in these two alloys are reported in section 3. The polyhedron topology statistics and the bond orientational order parameters corresponding to the simulated liquid structures are compared with those calculated in the cubic α-AlMnSi phase [9] and the model of AlMnSi relaxed quasicrystal [10], built from the model of Duneau and Oguey [11]. In these two descriptions, we examine more particularly the parameters characterizing the icosahedral order. Changes in the local symmetries when decreasing the temperature are then discussed from the undercooled liquid configurations obtained at 0.8 T_m by molecular dynamics. In section 4, we present refined simulated liquid configurations using the reverse Monte Carlo (RMC) method, which yield partial correlation functions in excellent agreement with the experimental curves. The local symmetries characterizing the RMC configurations are finally compared with those found in the MD configurations.

2. Interatomic potentials.

In order to obtain reliable descriptions of the structure of liquid $Al_{80}Mn_{20}$ and $Al_{80}Ni_{20}$ by the molecular dynamics method, we use interatomic pair potentials $\phi_{ij}(r)$ derived from our previous neutron diffraction data. They are calculated in the Percus-Yevick approximation [12] extended to binary systems, which from a previous study on the accuracy of the liquid theory approximate methods [13] appears to be more accurate than the hypernetted-chain equation in the region of the main peak :

$$\phi_{ij}(r) = k_B T \ln [1 - C_{ij}(r)/g_{ij}(r)] . \quad (1)$$

In equation (1), $C_{ij}(r)$ are the direct correlation functions which are of shorter range than $g_{ij}(r)$. They are obtained by Fourier transformation of the functions $\tilde{C}_{ij}(q)$ which are related to the experimental Ashcroft-Langreth partial structure factors $S_{ij}(q)$ [14] as follows :

$$\tilde{C}_{ii}(q) = (1 - S_{jj}(q) D(q))/n_i$$
$$\tilde{C}_{ij}(q) = S_{ij}(q) D(q)/\sqrt{n_i n_j} \quad (2)$$

with $$D(q) = 1/(S_{ii}(q) S_{jj}(q) - S_{ij}^2(q)) \quad \text{and} \quad n_i = c_i n .$$

c_i is the atomic concentration of species i and n the total number density.

The main difficulty for deriving reliable $\phi_{ij}(r)$ arises from the determination of $\tilde{C}_{ij}(q)$ at small scattering vectors. Small errors on $S_{ij}(q)$ yield large noise in the values of $\tilde{C}_{ij}(q)$ (as shown in Figs. 1 and 2). In order to improve the extraction of $\phi_{ij}(r)$ which are sensitive to the low-q part of $\tilde{C}_{ij}(q)$, the experimental points of $\tilde{C}_{ij}(q)$ derived from equation (2) have been smoothed from 0 to about 1 $Å^{-1}$ by forcing $\tilde{C}_{ij}(q)$ to tend at $q = 0$ towards the thermodynamic limit $\tilde{C}_{ij}(0)$, deduced from the limits $S_{ij}(0)$. The calculations of $S_{ij}(0)$ from the following thermodynamic quantities : the molar volume V_m, the isothermal compressibility K_T, and the limit $S_{CC}(0)$ (related to the Gibbs free energy), were presented in references [3] and [5] for $Al_{80}Mn_{20}$ and $Al_{80}Ni_{20}$.

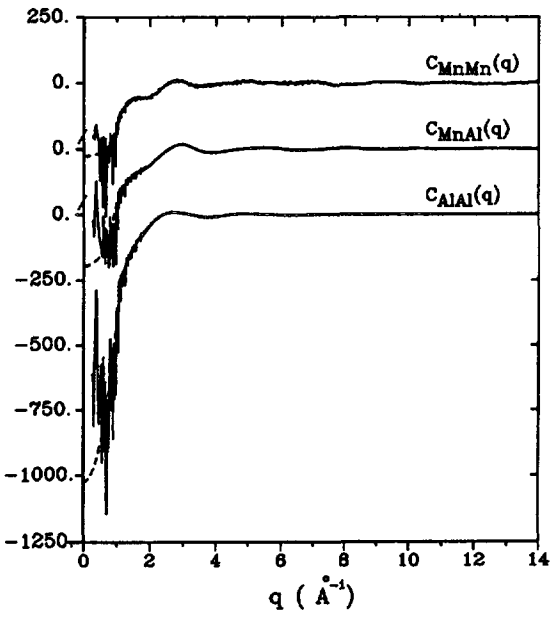

Fig. 1.

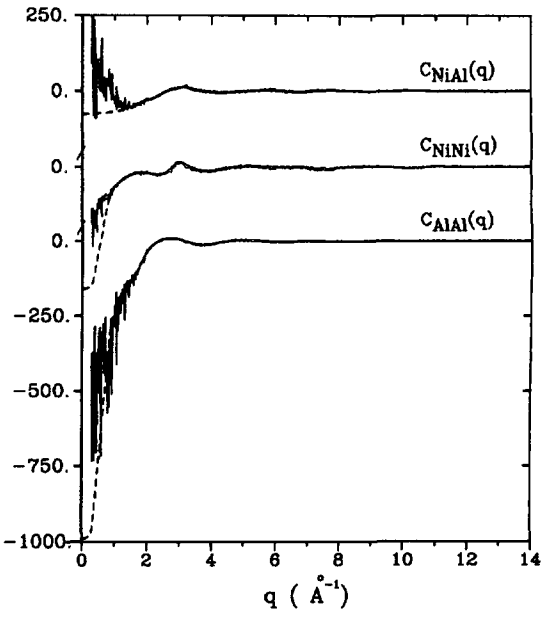

Fig. 2.

Fig. 1. — Partial functions $\tilde{C}_{ij}(q)$ for liquid $Al_{80}Mn_{20}$. (——) calculated from the experimental partial structure factors using equation (2), (-----) low-q parts smoothed towards the thermodynamic limits given in table I.

Fig. 2. — Partial functions $\tilde{C}_{ij}(q)$ for liquid $Al_{80}Ni_{20}$. (——) calculated from the experimental partial structure factors using equation (2), (-----) low-q parts smoothed towards the thermodynamic limits given in table I.

Thus, the accuracy in $\tilde{C}_{ij}(0)$ is limited by the experimental precision in the thermodynamic quantities. By way of illustration, we report in table I the errors in $\tilde{C}_{ij}(0)$ calculated starting with realistic errors of 1 % in V_m and K_T, and 5 % in $S_{CC}(0)$. While for the two liquids the relative errors in the limit $\tilde{C}_{AlAl}(0)$ of the majority atoms remain small, some of them can be very large such as in $\tilde{C}_{NiAl}(0)$. Several calculations of $\phi_{ij}(r)$ by changing the values of $\tilde{C}_{ij}(0)$ in the range given in table I have shown that for any atomic pair a decrease of

Table I. — *Thermodynamic limits of the functions* $\tilde{C}_{ij}(q)$ *for the liquid alloys* $Al_{80}Mn_{20}$ *and* $Al_{80}Ni_{20}$, M = Mn, Ni *(see also text).*

ATOMIC PAIR	$Al_{80}Mn_{20}$	$Al_{80}Ni_{20}$
M - M	- 277 (± 50)	- 410 ± 75
M - Al	- 450 (± 40)	- 76 ± 50
Al - Al	- 1032 (± 35)	- 992 ± 35

$\tilde{C}_{ij}(0)$ yields a more repulsive potential but does not change the general shape of $\phi_{ij}(r)$ significantly, and in particular its oscillations are not phase-shifted. We have checked that at low q the three pair partial structure factors are reconstructed in a satisfying way from the three adjusted parts of $\tilde{C}_{ij}(q)$. Our method appears to be more accurate than the method used by Li and Cowlam [15] to extract pair potentials for metallic glasses, which consists in extrapolating the three curves $S_{ij}(q)$ freehand down to $q = 0$ and then in calculating the $\tilde{C}_{ij}(q)$ functions.

The direct correlation functions $C_{ij}(r)$ are obtained by Fourier transformation of the adjusted functions $\tilde{C}_{ij}(q)$ such as :

$$C_{ij}(r) = \frac{1}{2\pi r^2} \int_0^{q_{max}} q\tilde{C}_{ij}(q) \sin(qr) \left[\exp\left(-\frac{q^2}{q_{max}^2} \ln A \right) \right] dq . \quad (3)$$

In integral (3) the exponential term is a damping factor of the oscillations of $\tilde{C}_{ij}(q)$ (for $A = 0.5$ the oscillations are decreased by a factor of 2 at q_{max}). The truncation values q_{max} in integral (3) are identical to those chosen for the calculation of $g_{ij}(r)$ from $S_{ij}(q)$ (see Refs. [3] and [5]).

The potentials $\phi_{ij}(r)$ using equation (1) are calculated from minimal distances such that $g_{ij}(r)$ are strictly positive. For $Al_{80}Mn_{20}$ these distances of 2.2 Å are identical for the three atomic pairs : for $Al_{80}Ni_{20}$ they are slightly different and equal to 2.1, 1.5 and 2.1 Å for the NiNi, NiAl and AlAl pairs, respectively. Since $g_{ij}(r)$ are positive, $\phi_{ij}(r)$ are calculable provided $C_{ij}(r)$ are smaller than $g_{ij}(r)$. From the functions $\tilde{C}_{ij}(q)$ adjusted at low q this condition is always satisfied, while it is not when the raw functions are used. This point also emphasizes the importance of the long-wavelength limits in the extraction of pair potentials which determine the slopes of $\tilde{C}_{ij}(q)$ at small q.

A damping factor was only applied for $Al_{80}Ni_{20}$. Indeed the function $g_{NiNi}(r)$ in reference [5] exhibits negative values beyond the first neighbour peak. Since $C_{NiNi}(r)$ is still lower in this region, $\phi_{NiNi}(r)$ cannot be derived. A means of removing this spurious effect due to the unaccuracy of $S_{NiNi}(q)$ is to use a damping factor similar to that used for $\tilde{C}_{NiNi}(q)$ in the calculation of the Fourier transform of $S_{NiNi}(q)$. In order to get comparable interatomic interactions for any atomic pair in the molecular dynamics simulations, the same damping factor (here $A = 0.3$) was used for the calculations of all the functions $g_{ij}(r)$ and $C_{ij}(r)$. The effect of such a factor is to reduce the amplitudes of the oscillations of $\phi_{ij}(r)$.

In figure 3, we present the interatomic potentials in $Al_{80}Mn_{20}$ and $Al_{80}Ni_{20}$ obtained from the adjusted functions $\tilde{C}_{ij}(q)$. They exhibit strong oscillations in the first neighbour region, then damp down rapidly beyond 6 Å. The first minima which are positive or negative correspond quite well to the first maximum positions of the experimental pair correlation functions shown in figures 4 and 5. For instance, in $\phi_{NiNi}(r)$ the two minima at 2.35 and 2.8 Å

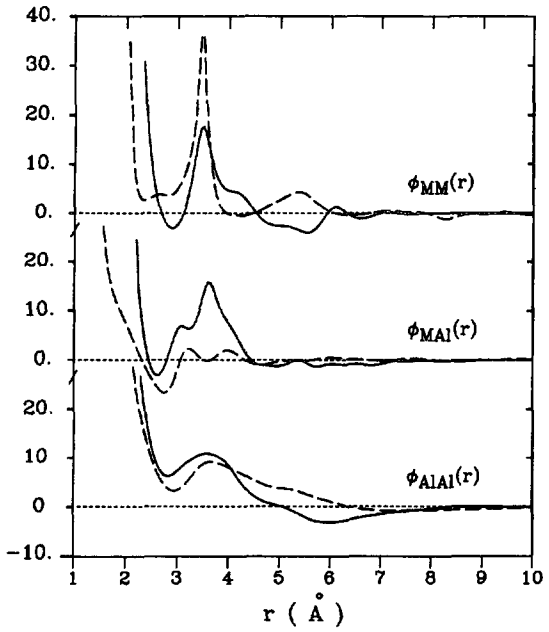

Fig. 3. — Interatomic pair potentials $\phi_{ij}(r)$ (in mRy) derived from diffraction data for liquid $Al_{80}Mn_{20}$ (——) and $Al_{80}Ni_{20}$ (----) (M = Mn or Ni).

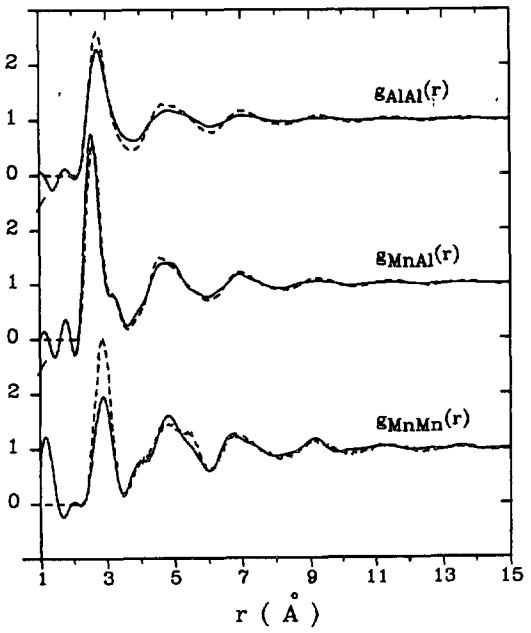

Fig.4.

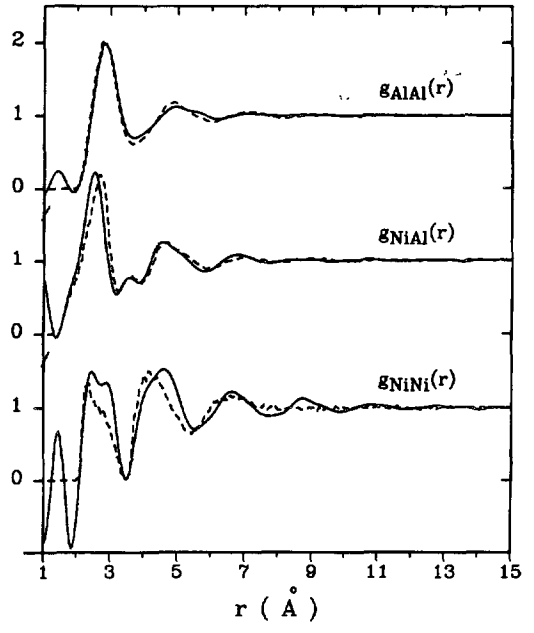

Fig.5.

Fig. 4. — Partial pair correlation functions $g_{ij}(r)$ obtained from neutron diffraction (——) and molecular dynamics (---) for liquid $Al_{80}Mn_{20}$.

Fig. 5. — Partial pair correlation functions $g_{ij}(r)$ obtained from neutron diffraction (——) and molecular dynamics (---) for liquid $Al_{80}Ni_{20}$.

reflect the two components in the distribution of the first neighbours NiNi. The strongly repulsive part of $\phi_{NiNi}(r)$ around 3.5 Å comes from the very small values of $g_{NiNi}(r)$ in this region. The most interesting feature is certainly the repulsive character of the potentials $\phi_{AlAl}(r)$ in the first neighbour region with the existence of a repulsive hump besides the repulsive core. For both liquids $\phi_{AlAl}(r)$ becomes attractive only at the upper limit of the second neighbour shell. It is worth emphasizing that, on the one hand, this shape of potential in the first neighbour region was already calculated by Duesbery *et al.* [16] for pure aluminium and was attributed to the choice of electron gas screening, on the other hand, the pair potential derived from Al liquid X-ray data [17] was also found positive up to 4.2 Å. Consequently, the pair potential $\phi_{AlAl}(r)$ for $Al_{80}Ni_{20}$ derived from our experimental results [5] seems to be more reliable than that extracted from neutron data using also the Percus-Yevick approximation in the same liquid alloy twenty years earlier [18], which presents a negative potential well in the first neighbour region.

3. Molecular dynamics simulations.

3.1 PROCEDURE. — The molecular dynamics simulations were carried out for a system of 691 Al atoms and 173 M atoms (M = Mn or Ni) in a cubic box with periodic boundary conditions at constant volume and constant temperature (T = 1 323 K for $Al_{80}Mn_{20}$ and $Al_{80}Ni_{20}$) with constrained equations of motions [19]. The size of the box is chosen in such a way that the density of the 864 particles' systems is equal to that of the liquid (n = 0.058 at/Å^3 for $Al_{80}Mn_{20}$ and 0.06 at/Å^3 for $Al_{80}Ni_{20}$). The initial atomic positions are randomly chosen with the constraint of a minimal interatomic distance of 2.2 Å, together with a Gaussian distribution of initial velocities, such that the mean kinetic energy corresponds to the chosen temperature. The instantaneous forces on each particle due to its neighbours are computed from the interatomic potentials described in section 2. The potentials $\phi_{ij}(r)$ are represented by cubic splines. They are set to zero from of the nodes beyond which the oscillations of $\phi_{ij}(r)$ are largely damped down. The truncation values for the atomic pairs MM, MAl and AlAl are equal to 6, 5.4 and 5.1 Å for $Al_{80}Mn_{20}$ and 6.1, 5.7 and 6.5 Å for $Al_{80}Ni_{20}$, respectively.

For $Al_{80}Mn_{20}$ a total of 80 000 molecular dynamics time steps (t_s = 1.5 10^{-16} s) have been performed ; the instantaneous potential energy E_p of the system has attained its equilibrium value after roughly 20 000 steps, beyond E_p fluctuates around this mean value. For $Al_{80}Ni_{20}$, 160 000 steps have been realized and the system tends towards its equilibrium configuration after 60 000 steps. For both liquids, the pressure of the 864 particles' system in the equilibrium state remains considerably high ($p \approx 10^5$ atm) and could be attributed to the fact that only the repulsive part of the potential $\phi_{AlAl}(r)$ is taken into consideration in the calculation of the interatomic forces.

3.2 PARTIAL PAIR CORRELATION FUNCTIONS. — The calculated pair correlation functions, shown in figures 4 and 5, are the curves averaged over 60 configurations taken among the last 60 000 steps for $Al_{80}Mn_{20}$ and 100 configurations among the last 100 000 steps for $Al_{80}Ni_{20}$ at intervals of 1 000 steps. For both liquids, the overall agreement between experiment and molecular dynamics calculations is rather good. Small features such as the shoulder at the right side of the first peak of $g_{MnAl}(r)$, the asymmetry of the first peak in $g_{NiAl}(r)$ and the double-component first peak in $g_{NiNi}(r)$ are well reproduced. However, for $Al_{80}Mn_{20}$ some differences in the intensities of the first peaks in $g_{AlAl}(r)$ and $g_{MnMn}(r)$ are observed, and for $Al_{80}Ni_{20}$ a phase-shift between the experimental and calculated curves for $g_{NiNi}(r)$ appears in the second-neighbour region nevertheless.

3.3 NUMBER-NUMBER STRUCTURE FACTOR. — In figures 6 and 7, we present the calculated number-number structure factors $S_{NN}(q)$ obtained by inverse Fourier transformation of the corresponding $g_{NN}(r)$ functions together with the experimental curves. For both liquids, the overall agreement is satisfying. In the same manner as for the $g_{ij}(r)$'s, for $Al_{80}Mn_{20}$ both experimental and calculated curves are perfectly in phase, while for $Al_{80}Ni_{20}$ a phase-shift exists from the second peak. The adjustments of the $\tilde{C}_{ij}(q)$ functions at low q force the calculated $S_{NN}(q)$ function for $Al_{80}Ni_{20}$ to tend towards its correct thermodynamic value of 0.046. The most interesting feature is the splitting of the second peak for $Al_{80}Mn_{20}$ at positions close to $1.7\,q_1$ and $2\,q_1$ ($q_1 = 2.86$ Å^{-1}) which is well resolved by molecular dynamics and suggestive of local icosahedral order. By contrast, for $Al_{80}Ni_{20}$ the calculated

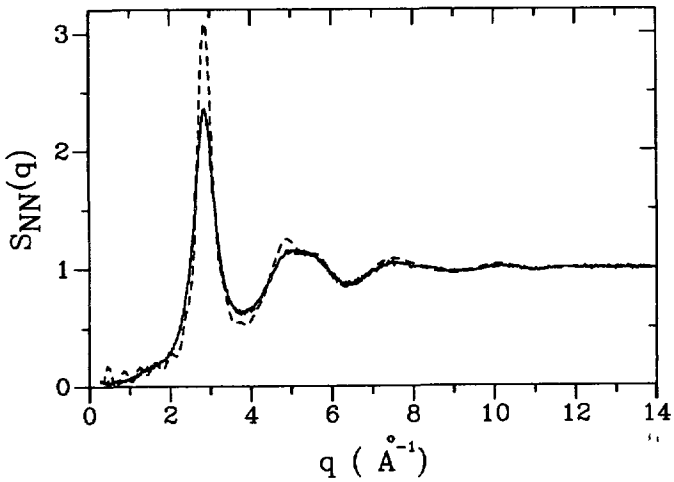

Fig. 6. — Number-number structure factors $S_{NN}(q)$ obtained from neutron diffraction (——) and molecular dynamics (---) for liquid $Al_{80}Mn_{20}$.

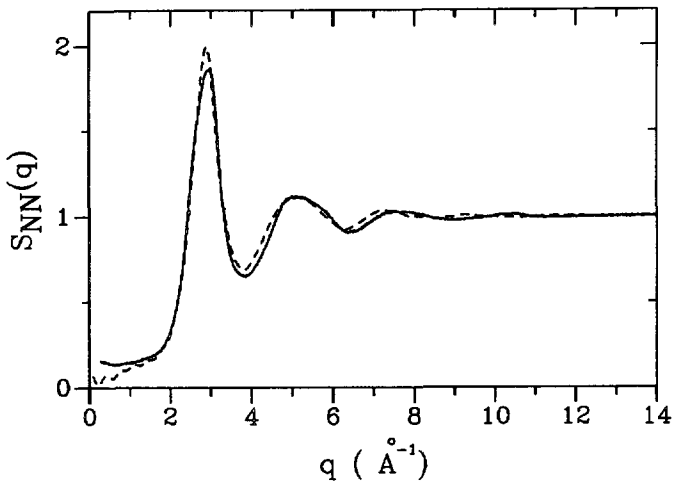

Fig. 7. — Number-number structure factors $S_{NN}(q)$ obtained from neutron diffraction (——) and molecular dynamics (---) for liquid $Al_{80}Ni_{20}$.

curve exhibits a rounded second peak similar to that of the experimental curve. As will be shown in the next section, these features are consistent with the analyses of local symmetries.

3.4 CHARACTERIZATION OF THE LOCAL SYMMETRIES. — Two methods of determining and representing the local symmetries in liquid $Al_{80}Mn_{20}$ and $Al_{80}Ni_{20}$ are presented. The first method is based on the Voronoï polyhedron topology statistics and the second method is derived from the calculations of the bond orientational order parameters Q_ℓ. The results obtained for the quasicrystal forming liquid $Al_{80}Mn_{20}$ are compared with those calculated in the crystalline α-AlMnSi phase [9] and the AlMnSi relaxed icosahedral quasicrystal model [10].

3.4.1 *Voronoi polyhedra.* — The description of the topology in terms of Voronoï polyhedra was first made in dense random packing models for simple liquids [20]. For random packings of two species with different sizes, the radical plane method proposed by Gellatly and Finney [21] was better adapted and applied to metallic glasses. In $Al_{80}Mn_{20}$ and $Al_{80}Ni_{20}$ liquids, since the two atomic species have close atomic radii, the construction of Voronoï polyhedra is preferentially chosen. As will be shown, the decomposition into radical (Laguerre) polyhedra leads to similar results.

Each Voronoï polyhedron constructed around an atom is defined by a set of integers $(n_3, n_4, n_5, \ldots, n_i, \ldots)$ where n_i represents the number of faces having i edges. Each face of every polyhedron bisects a near neighbour bond and thus the number of faces of the polyhedron defines a number of first neighbours around the central atom. The Voronoï polyhedron statistics in $Al_{80}Mn_{20}$ have been made up from 60 configurations taken among the last 60 000 steps at intervals of 1 000 steps and in $Al_{80}Ni_{20}$ from 100 configurations among the last 100 000 steps at the same interval. The types and percentages of the most frequently observed polyhedra are presented in table II together with those calculated in the icosahedral quasicrystal model and the α phase, we also give the 1 % confidence interval on each percentage. Note that for a given configuration, by partitioning into radical polyhedra (using

Table II. — *Types and percentages of the most frequent Voronoi polyhedra found in the simulated* $Al_{80}Mn_{20}$ *and* $Al_{80}Ni_{20}$ *liquids, in the relaxed icosahedral quasicrystal model and in the cubic* α-AlMnSi *phase. The common polyhedron types between liquid* $Al_{80}Mn_{20}$ *and the other phases are exposed in heavy characters.*

Liquid $Al_{80}Mn_{20}$ 1320K - MD		**Relaxed icosahedral quasicrystal model**		**Cubic α-AlMnSi phase**		**Liquid $Al_{80}Ni_{20}$ 1320K - MD**	
$(n_3,n_4,n_5,n_6,)$	pct	$(n_3,n_4,n_5,n_6,)$	pct	$(n_3,n_4,n_5,n_6,)$	pct	$(n_3,n_4,n_5,n_6,)$	pct
(0,3,6,4)	**4.1±0.2**	(0,3,6,6)	7.1	(0,4,8,1)	17.4	**(0,3,6,4)**	**2.1±0.15**
(0,1,10,2)	**4.05±0.25**	**(0,3,6,5)**	**6.2**	(0,3,10,1)	17.4	**(0,2,8,4)**	**1.3±0.1**
(0,2,8,4)	**3.8±0.2**	**(0,2,8,4)**	**5.8**	**(0,0,12)**	**13.**	(1,3,4,5,1)	1.25±0.1
(0,2,8,2)	**2.8±0.2**	**(0,0,12)**	**5.6**	(0,2,8,1)	8.7	**(0,3,6,5)**	**1.2±0.1**
(0,0,12)	**2.3±0.2**	(0,4,4,7)	3.1	**(0,2,8,4)**	**8.7**	(0,4,5,4,1)	1.1±0.1
(0,3,6,5)	**2.0±0.15**	**(0,3,6,4)**	**2.8**	(1,7,3,1)	8.7	**(1,2,6,3,1)**	**1.1±0.1**
(0,1,10,3)	**1.8±0.2**	**(0,1,10,3)**	**2.7**	(4,3,4)	8.7	**(0,3,6,3)**	**1.1±0.1**
(0,2,8,5)	**1.7±0.15**	**(0,2,8,5)**	**2.6**	(0,2,10,1)	8.7	(1,3,5,3,2)	1.05±0.1
(0,3,6,3)	**1.6±0.15**	(0,4,4,8)	2.5	(0,3,10,2)	4.4	(1,3,4,4,1)	1.0±0.1
(0,2,8,3)	1.6±0.2	**(0,1,10,2)**	**2.5**	(0,2,12,1)	4.4	(0,3,7,4,1)	1.0±0.1
(1,2,6,3,1)	**1.5±0.1**	(0,2,8,1)	2.1			**(0,2,8,2)**	**1.0±0.1**
						•	
						(0,0,12)	**0.2±0.05**

atomic radii equal to 2.82 Å and 2.5 Å for Al and transition metal atoms respectively) we obtain the same types of the most frequently observed polyhedra with similar percentages.

The population of atoms with icosahedral symmetry characterized by the pentagonal dodecahedron (0, 0, 12) is of 13 % in the α-phase, 5.6 % in the icosahedral model, 2.3 % in liquid $Al_{80}Mn_{20}$ and only 0.2 % in $Al_{80}Ni_{20}$. Moreover, among the polyhedra listed in table II, seven of them are observed in both the liquid $Al_{80}Mn_{20}$ and the icosahedral model ; by taking the corresponding lowest percentages, we find that at least 17 % of the atomic sites have the same local symmetry. In contrast, only two types of polyhedra found in the α-phase are also observed in the liquid $Al_{80}Mn_{20}$ representing 6.1 % of atomic sites.

Even if the proportion of (0, 0, 12) polyhedra in the liquid $Al_{80}Mn_{20}$ is small, the importance of local icosahedral order must not be underestimated, especially in comparison with the almost zero proportion found in $Al_{80}Ni_{20}$. By counting the first neighbours of the atomic sites with icosahedral symmetry, 22 % of the 864 atoms are engaged in such order and in average the icosahedra are connected two by two. Consequently, there is no chain of icosahedral clusters, as it was proposed in the liquid eutectic AgGe to explain the small angle neutron scattering signal [22].

The three polyhedron types constructed in the crystalline phase Al_3Ni [23], the nearest compound from the liquid composition $Al_{80}Ni_{20}$, are the following ones : (0, 3, 6, 5), (0, 3, 6) and (0, 3, 6, 8) with respective frequencies of 50 %, 25 % and 25 %. The (0, 3, 6) polyhedron type constructed around Ni atoms characterizes a trigonal prismatic neighbourhood. According to table II, only the (0, 3, 6, 5) polyhedron also belongs to the list of the first 11 polyhedra found in the liquid $Al_{80}Ni_{20}$ but with a frequency of 1.3 % still lower than in $Al_{80}Mn_{20}$. The types of bond-orientational order in the Al_3Ni compound have, therefore, almost completely disappeared in the liquid $Al_{80}Ni_{20}$. Indeed, there are more similarities between the two liquid structures, since at least 8 % of the atomic sites have similar local symmetries. The distribution of the polyhedron types much more spread out in $Al_{80}Ni_{20}$ than in $Al_{80}Mn_{20}$ indicates essentially that the local topological order in liquid $Al_{80}Ni_{20}$ is less defined than in $Al_{80}Mn_{20}$.

3.4.2 *Bond-orientational order parameters.* — Another way of characterizing the local symmetries has been developed by Steinhardt *et al.* [2] to study the bond-orientational order in Lennard-Jones supercooled liquids. To every bond joining a central particle to one of its neighbours, they associate a spherical harmonic :

$$Q_{\ell m}(\mathbf{r}) = Y_{\ell m}(\theta(\mathbf{r}),\ \phi(\mathbf{r}))\,, \tag{4}$$

where θ and ϕ are the polar angles of the bond represented by the vector $\mathbf{r}$.

To each atom surrounded by N near neighbours, correspond average values of $Q_{\ell m}(\mathbf{r})$:

$$\bar{Q}_{\ell m} = \frac{1}{N} \sum_{i} Y_{\ell m}(\theta_i,\ \phi_i)\,. \tag{5}$$

Since $\bar{Q}_{\ell m}$ changes for a given ℓ if one rotates the coordinate system, Steinhardt *et al.* had the idea to calculate the second-order invariants such as :

$$Q_\ell = \left[\frac{4\pi}{2\ell + 1} \sum_{m=-\ell}^{\ell} \left| \bar{Q}_{\ell m} \right|^2 \right]^{1/2} \tag{6}$$

and they found that the sequences $\{Q_\ell\}$ were characteristics of cluster symmetries. For instance, clusters with icosahedral symmetry exhibit nonzero bond-orientational order parameters for $\ell = 6,\ 10,\ 12$. Here, the bond-orientational order parameters which will

characterize the symmetries of the simulated liquids will be finally obtained by averaging the values of Q_ℓ over all the particles of different equilibrium configurations.

To calculate the parameters Q_ℓ, we need to define the number N of near neighbour atoms in equation (5). We restrict the analysis of Q_ℓ to the local scale, i.e. for the $Al_{80}Mn_{20}$ and $Al_{80}Ni_{20}$ simulated liquids we consider around any atom all the neighbours within the first coordination shell of radius r_{min}. The value of r_{min} is chosen such that the average number of first neighbours is close to 12 (r_{min} is equal to 3.75 and 3.7 Å for $Al_{80}Mn_{20}$ and $Al_{80}Ni_{20}$ respectively, and corresponds roughly to the position of the first minimum in the Fourier transform of $S_{NN}(q)$). In the icosahedral and α phases, r_{min} is taken equal to 3.7 Å giving coordination numbers of 12.2 and 12.7 respectively. Figure 8 shows the histogram of Q_ℓ *versus* ℓ up to $\ell = 12$ for liquid $Al_{80}Mn_{20}$ and $Al_{80}Ni_{20}$, the relaxed icosahedral quasicrystal and the α-phase. For each ℓ number, Q_ℓ are the values averaged over the 864 particles of the liquid structures, the 10 028 particles of the quasicrystal model and the 138 atoms of the α-phase. For the liquids, the values of Q_ℓ corresponding to the random initial configuration are shown together with close calculated from the equilibrium configurations which are the values averaged over 6 configurations taken among the last 60 000 steps at intervals of 10 000 steps for $Al_{80}Mn_{20}$, and 10 configurations among the last 100 000 steps at the same interval for $Al_{80}Ni_{20}$. Most of the values for the perfect 13-atom icosahedral cluster fall out of the range of figure 8 and are not shown (for $\ell = 6$, 10, 12 the Q_ℓ's are equal to 0.663, 0.363 and 0.585).

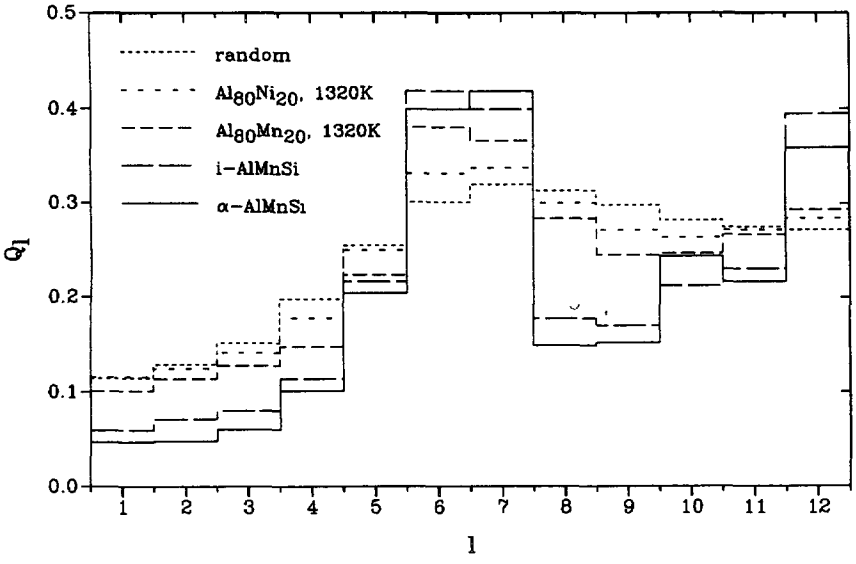

Fig. 8. — Second-order invariants Q_ℓ for the initial and equilibrium configurations of the simulated $Al_{80}Mn_{20}$ and $Al_{80}Ni_{20}$ liquids, the relaxed icosehedral AlMnSi quasicrystal model and the α-AlMnSi phase.

Except for $\ell = 10$, the even values of Q_ℓ for the quasicrystal model and the α-phase stand between those for the liquids and the 13-atom icosahedral cluster. For any ℓ number, the changes in Q_ℓ between the initial and equilibrium states are larger for $Al_{80}Mn_{20}$ than for $Al_{80}Ni_{20}$, such that the equilibrium values for $Al_{80}Mn_{20}$ are approaching closer to the values of the icosahedral model or the α-phase. In particular, the icosahedral symmetry is more

developed in $Al_{80}Mn_{20}$ than in $Al_{80}Ni_{20}$, as suggested by the strong difference between the equilibrium values of Q_6.

3.5 MOLECULAR DYNAMICS SIMULATIONS OF $Al_{80}Mn_{20}$ AND $Al_{80}Ni_{20}$ SUPERCOOLED LIQUIDS. — In order to follow the changes in the local symmetries when decreasing the temperature, molecular dynamics simulations of supercooled liquids, $Al_{80}Mn_{20}$ and $Al_{80}Ni_{20}$, were performed at 1 000 K (i.e. 0.8 T_m) using the same interatomic potentials as shown in figure 3. We started from the final 864-particle configuration obtained at 1 320 K by molecular dynamics and we associated a new Gaussian distribution of velocities such that the kinetic energy corresponds to a temperature of 1 000 K. For the two alloys, 100 000 molecular time steps were performed at constant temperature and pressure ; the pressure being chosen equal to that obtained by simulation at 1 320 K. The enthalpy of the system ($E_p + PV$) has attained its equilibrium value after 60 000 steps for $Al_{80}Mn_{20}$ and 40 000 steps for $Al_{80}Ni_{20}$.

The Voronoï polyhedron statistics were compiled from 50 independent equilibrium configurations taken among the last 50 000 ones at intervals of 1 000 steps for $Al_{80}Mn_{20}$ and 70 configurations among the last 70 000 at the same interval for $Al_{80}Ni_{20}$. In table II are presented the most frequently observed types of Voronoï polyhedra in the undercooled liquids together with those found in a dense random packing model of amorphous iron [24]. It is remarkable that the five most frequent types of polyhedra are identical in the undercooled liquid $Al_{80}Mn_{20}$ and in the amorphous iron model. It is worth recalling that in this amorphous iron model, Srolovitz *et al.* have shown through the calculations of local structural parameters that, on the one hand, all the polyhedra presented a degree of ellipsoidal deviation from the spherical symmetry of the environment, and on the other hand, the (0, 0, 12) polyhedra were located in the most compressive regions [24].

Now, by comparing the results given in tables II and III, we can observe that for $Al_{80}Mn_{20}$ the five most frequent types of polyhedra found at 1 000 K are identical with those found at higher temperatures. In contrast, for $Al_{80}Ni_{20}$ the statistics are quite different since two new

Table III. — *Types and percentages of the most frequent Voronoi polyhedra found in the simulated undercooled liquids of* $Al_{80}Mn_{20}$ *and* $Al_{80}Ni_{20}$, *and in a random packing model of amorphous iron* [24]. *The common polyhedron types between the undercooled liquid* $Al_{80}Mn_{20}$ *and the other phases are expressed in heavy characters.*

Undercooled liquid $Al_{80}Mn_{20}$		**Undercooled liquid $Al_{80}Ni_{20}$**		**Random packing model of amorphous iron**	
$(n_3,n_4,n_5,n_6,)$	pct	$(n_3,n_4,n_5,n_6,)$	pct	$(n_3,n_4,n_5,n_6,)$	pct
(0,1,10,2)	**6.9±0.3**	**(0,3,6,4)**	**3.1±0.2**	**(0,1,10,2)**	**13**
(0,2,8,4)	**5.7±0.3**	**(0,2,8,4)**	**2.5±0.2**	**(0,3,6,4)**	**8.8**
(0,0,12)	**4.9±0.2**	**(0,3,6,5)**	**1.9±0.15**	**(0,0,12)**	**8.7**
(0,3,6,4)	**4.8±0.25**	**(0,1,10,2)**	**1.8±0.15**	**(0,2,8,2)**	**7.5**
(0,2,8,2)	**3.8±0.25**	**(0,2,8,2)**	**1.8±0.15**	**(0,2,8,4)**	**4.6**
(0,1,10,3)	3.5±0.2	(1,3,4,5,1)	1.5±0.1	(0,3,6,3)	4.2
(0,3,6,5)	**2.6±0.2**	(0,3,6,3)	1.4±0.1	(0,0,12,2)	3.2
(0,2,8,5)	**2.5±0.2**	(1,2,6,3,1)	1.4±0.1		
(0,1,10,4)	2.2±0.2	**(0,2,8,5)**	**1.3±0.1**		
(1,0,9,3)	2.0±0.2	(0,3,7,4,1)	1.3±0.1		
		•			
		(0,0,12)	**0.7±0.1**		

types of polyhedra, (0, 1, 10, 2) and (0, 2, 8, 2), appear at 1 000 K among the five most frequent ones. Moreover, icosahedral symmetry increases significantly for $Al_{80}Mn_{20}$ and starts to develop in $Al_{80}Ni_{20}$. On the whole, for $Al_{80}Mn_{20}$ the main types of local symmetry found at 1 323 K are preserved at lower temperatures, while for $Al_{80}Ni_{20}$ the atomic rearrangements are more significant.

The second-order invariants were averaged over 5 configurations taken among the last 50 000 ones at intervals of 10 000 steps for $Al_{80}Mn_{20}$ and 7 configurations among the last 70 000 ones at the same interval for $Al_{80}Ni_{20}$. Figure 9 shows the effect of temperature on the invariants Q_ℓ, which except for $\ell = 5$ is similar for the two alloys : i.e. when decreasing the temperature, the Q_ℓ-values of the supercooled liquids are approaching closer to the values corresponding to the icosahedral phase model. In particular, the increase of Q_ℓ for $\ell = 6$ is well pronounced in agreement with the higher percentages of atoms with icosahedral symmetry.

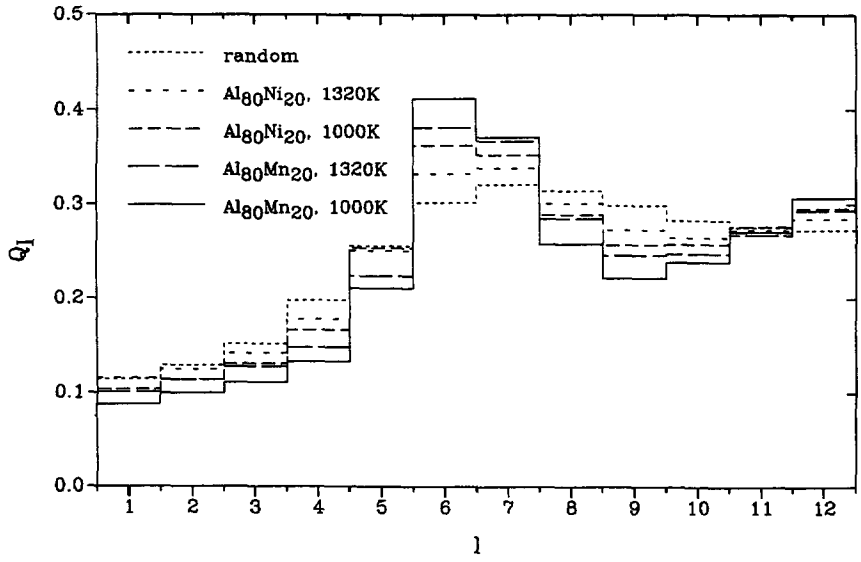

Fig. 9. — Effect of the temperature on the second-order invariants Q_ℓ for the simulated $Al_{80}Mn_{20}$ and $Al_{80}Ni_{20}$ liquids. The Q_ℓ values for the initial random configuration are also presented.

4. Reverse Monte Carlo simulations of liquid $Al_{80}Mn_{20}$ and $Al_{80}Ni_{20}$.

In section 3, we have seen that the liquid configurations simulated by molecular dynamics yielded a good, but not perfect, representation of the experimental functions. Consequently, information on the local symmetries extracted from these configurations contains some unaccuracy difficult to estimate.

A way of generating configurations which allows a good representation of diffraction data is the so-called reverse Monte Carlo method [25]. If we start with the final configuration obtained by molecular dynamics and let $g_{ij}(r)$ be the pair correlation functions of a configuration at a given step, a new configuration is generated by random motion of one particle among the 864 particles with a maximal displacement chosen equal to 0.1 Å.

If the particle in motion approaches any other particle within a distance smaller than the lower cutoff distances r_{ij}^0, taken equal to the first values for which the experimental $g_{ij}^E(r)$'s are non-zero, the new configuration is automatically rejected. Otherwise, the new configuration with the new pair correlation functions $g'_{ij}(r)$'s is accepted using a standard χ^2 test such as :

$$\chi^2 = \sum_{ij} \sum_{k=1}^{n} \frac{(g_{ij}^E(r_k) - g_{ij}(r_k))^2}{\sigma_{ij}^2} \tag{7}$$

and

$$\chi'^2 = \sum_{ij} \sum_{k=1}^{n} \frac{(g_{ij}^E(r_k) - g'_{ij}(r_k))^2}{\sigma_{ij}^2},$$

where n is the number of r points and σ_{ij} are the errors on the experimental curves $g_{ij}^E(r_k)$. If $\chi' < \chi$, the new configuration is accepted ; if $\chi' > \chi$, it is accepted with a probability that follows a normal distribution. The process is repeated until χ^2 decreases to an equilibrium value and then oscillates about it.

The $g_{ij}(r)$ functions are calculated with a path of 0.1 Å up to $L/2$ (L being the size of the box, equal to 24.6 Å for $Al_{80}Mn_{20}$ and 24.3 Å for $Al_{80}Ni_{20}$). The lower cutoff distances are equal to 2.2 Å for the three pairs in $Al_{80}Mn_{20}$, and 2.1 Å for AlAl and NiNi pairs and 1.5 Å for AlNi pairs in $Al_{80}Ni_{20}$. The experimental errors σ_{ij} are assumed constant ; for the two alloys they are equal to 0.02 for $g_{AlAl}(r)$ and 0.04 for $g_{AlM}(r)$ and $g_{MM}(r)$ (M = Mn or Ni).

The convergence is attained after about 65 000 accepted moves. Figures 10 and 11 show the calculated pair correlation functions, which are averaged over eight configurations taken

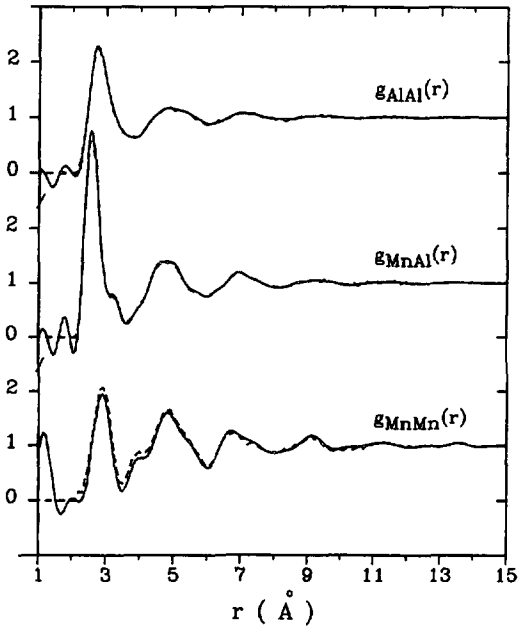

Fig. 10.

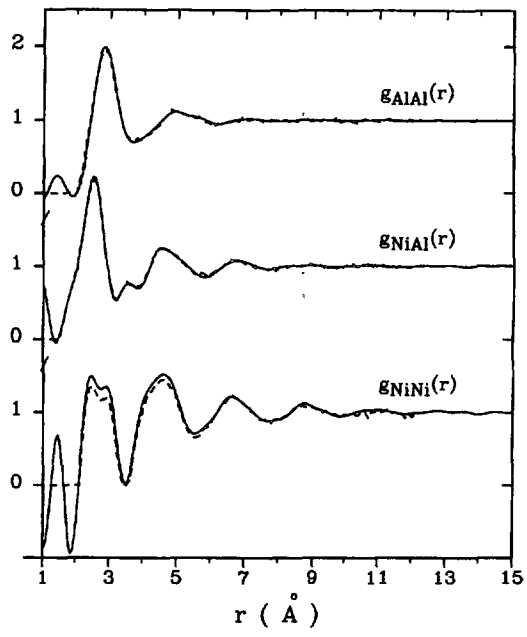

Fig. 11.

Fig. 10. — Partial pair correlation functions $g_{ij}(r)$ obtained from neutron diffraction (——) and reverse Monte Carlo (---) for liquid $Al_{80}Mn_{20}$.

Fig. 11. — Partial pair correlation functions $g_{ij}(r)$ obtained from neutron diffraction (——) and reverse Monte Carlo (---) for liquid $Al_{80}Ni_{20}$.

among those generated after 65 000 to 300 000 accepted moves. The agreement with the experimental curves is perfect for the AlAl and AlM pairs, and in comparison with the curves generated by molecular dynamics is clearly better for the MnMn and NiNi pairs.

The statistics of the Voronoï polyhedra established from the same configurations as those used for the calculations of the $g_{ij}(r)$ functions are presented in table IV. Due to the limited number of configurations, the 1 % confidence intervals on the percentages are wider than those found in the MD configurations. For the two liquids, most polyhedra which were among the ten most frequently occurring polyhedra in the MD configurations are always present (indicated in bold characters in Tab. IV) with respective percentages systematically lower. For $Al_{80}Mn_{20}$ we observe a significant decrease of the fractions of the (0, 1, 10, 2) and (0, 0, 12) polyhedron types. For $Al_{80}Ni_{20}$ the percentage of (0, 0, 12) polyhedra, already very weak in the MD configurations, also decreases in the RMC configurations. It appears that the most compressive regions, where from Srolovitz *et al.* [24] the 13-atom icosahedra are located, tend to decrease in the configurations generated by reverse Monte Carlo.

Table IV. — *Types and percentages of the most frequent Voronoi polyhedra found in the* $Al_{80}Mn_{20}$ *and* $Al_{80}Ni_{20}$ *liquid configurations generated by the reverse Monte Carlo method. The polyhedra common with the polyhedra the most frequently observed in the* $Al_{80}Mn_{20}$ *and* $Al_{80}Ni_{20}$ *liquids simulated by molecular dynamics are expressed in heavy characters.*

Liquid $Al_{80}Mn_{20}$ 1320K - RMC		Liquid $Al_{80}Ni_{20}$ 1320K -RMC	
$(n_3,n_4,n_5,n_6,)$	pct	$(n_3,n_4,n_5,n_6,)$	pct
(0,3,6,4)	**3.1±0.7**	**(0,3,6,4)**	**1.5±0.4**
(0,2,8,4)	**2.6±0.5**	**(0,2,8,4)**	**1.1±0.6**
(0,2,8,2)	**2.4±0.6**	**(1,2,6,3,1)**	**1.1±0.5**
(0,1,10,2)	**2.2±0.2**	**(1,3,4,5,1)**	**1.1±0.6**
(0,3,6,5)	**1.7±0.4**	**(1,3,4,4,1)**	**1.±0.5**
(1,3,4,5,1)	1.6±0.4	**(0,4,5,4,1)**	**1.±0.3**
(0,3,6,3)	**1.5±0.7**	(1,3,5,4,2)	0.9±0.5
(1,2,6,3,1)	**1.4±0.7**	**(0,3,6,5)**	**0.9±0.4**
(0,3,6,6)	1.3±0.7	**(0,3,7,4,1)**	**0.8±0.4**
(0,4,5,4,1)	1.3±0.5	(1,2,6,4,1)	0.8±0.4
	•		•
(0,0,12)	**1±0.3**	**(0,0,12)**	**0.04±0.05**

Figure 12 presents the histograms of Q_ℓ, these values are averaged over the same configurations as those previously used for the determination of the Voronoï polyhedra, in comparison with the histograms corresponding to the random configuration and the MD equilibrium configurations. We observe the same behaviour for the two alloys, i.e. globally the values of the RMC configurations are closer of the Q_ℓ's of the random configurations than the Q_ℓ's of the MD configurations. These results are consistent with the larger dispersion of the Voronoï polyhedron found in the RMC configurations than in the MD configurations.

Consequently, it turns out that the configurations generated by RMC are sensitively more disordered than the equilibrium configurations obtained by molecular dynamics. Even if the amount of icosahedral order has decreased in liquid $Al_{80}Mn_{20}$ after the RMC simulations, these simulations confirm the existence of a premonitory local icosahedral order in liquid $Al_{80}Mn_{20}$ in comparison with liquid $Al_{80}Ni_{20}$, which could explain the formation of the icosahedral $Al_{80}Mn_{20}$ phase.

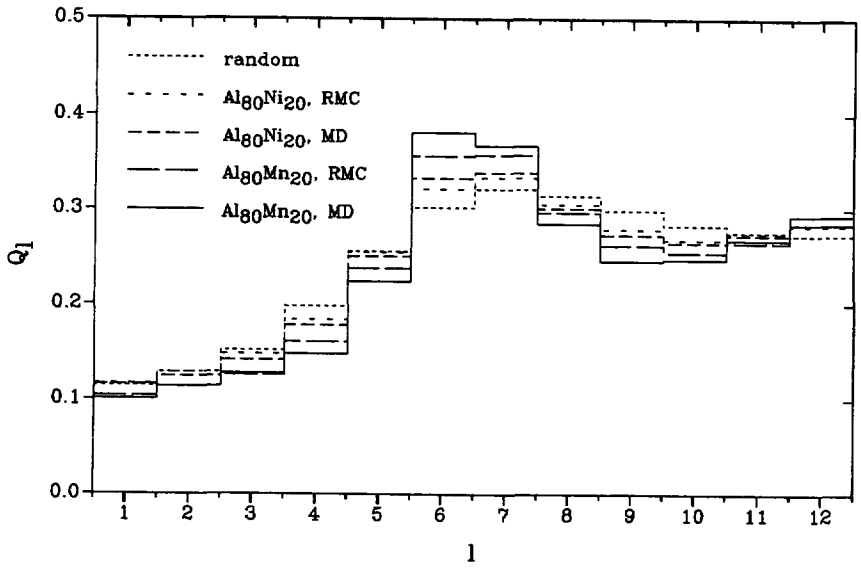

Fig. 12. — Comparison of the second-order invariants Q_ℓ for the molecular dynamics (MD) configurations of liquid $Al_{80}Mn_{20}$ and $Al_{80}Ni_{20}$ with those obtained in the reverse Monte Carlo (RMC) configurations at 1320 K. The Q_ℓ values for the initial random configuration are also given.

5. Conclusion.

For both liquid alloys $Al_{80}Mn_{20}$ and $Al_{80}Ni_{20}$, the rather good agreement between the experimental partial pair correlation functions and those calculated by the molecular dynamics technique gives some reliability in the interatomic potentials derived from our neutron diffraction experiments.

The characterization of the local symmetries from the calculation of the invariants of spherical harmonics and especially from the construction of the Voronoï polyhedra allows us to confirm the existence of a local icosahedral order in the quasicrystal forming liquid $Al_{80}Mn_{20}$. Even if it concerns only a small percentage of atoms, equal to 2.3 %, it is nevertheless significant in comparison with the percentage about ten times smaller found in $Al_{80}Ni_{20}$ which forms no quasicrystal.

The molecular dynamics simulations of the undercooled liquids show that for $Al_{80}Mn_{20}$ the most frequently occurring local symmetries observed above the liquidus line are not only preserved at 0.8 T_m but also more pronounced. For $Al_{80}Ni_{20}$, the atomic rearrangements are more considerable, since new symmetries appear among the most frequent ones, and in particular the icosahedral symmetry starts to develop.

The improvement of the agreement between the experimental partial pair correlation functions and those calculated by the reverse Monte Carlo method leads to $Al_{80}Mn_{20}$ and $Al_{80}Ni_{20}$ configurations which are, in average, more disordered than those generated by molecular dynamics. Nevertheless, they present the same most frequently observed symmetries as those obtained in the molecular dynamics configurations, yet with lower percentages.

Acknowledgments.

We are indebted to Dr M. A. Howe and Dr R. L. McGreevy for providing the reverse Monte Carlo programs.

References

[1] Shechtman D., Blech I., Gratias D., Cahn J. W., *Phys. Rev. Lett.* **53** (1984) 1951.
[2] Steinhardt J. P., Nelson D. R., Ronchetti M., *Phys. Rev. B* **28** (1983) 784.
[3] Maret M., Pasturel A., Senillou C., Dubois J. M., Chieux P., *J. Physique* **50** (1989) 295.
[4] Maret M., Chieux P., Dubois J. M., Pasturel A., *J. Phys. . Condensed Matter* **3** (1991) 2801.
[5] Maret M., Pomme T., Pasturel A., Chieux P., *Phys. Rev. B* **42** (1990) 1598.
[6] Sachdev S., Nelson D. R., *Phys. Rev. Lett.* **53** (1984) 1947.
[7] Bhatia A. B., Thornton D. E., *Phys. Rev. B* **2** (1970) 3004.
[8] Maret M., Lançon F., Billard L., *Physica B* **180/181** (1992) 854.
[9] Cooper M., Robinson K., *Acta Crystallogr.* **20** (1966) 614.
[10] Lançon F., Billard L., *J. Physique* **51** (1990) 1099.
[11] Duneau M., Oguey C., *J. Physique* **50** (1989) 135.
[12] Percus J. K., Yevick G. J., *Phys. Rev.* **110** (1958) 1.
[13] Bratkovsky A. M., Vaks V. G., Trefilov A. V., *J. Phys. F : Met. Phys.* **12** (1982) 611.
[14] Ashcroft N. W., Langreth D. C., *Phys. Rev.* **156** (1967) 685.
[15] Li J. C., Cowlam N., *Phys. Chem. Liq* **17** (1987) 29.
[16] Duesbery M. S., Taylor R., *Phys. Rev. B* **7** (1973) 2870.
[17] Ruppersberg H., Wehr H., *Phys. Lett. A* **40** (1972) 31.
[18] Enderby J. E., Howells W. S., Interatomic potentials and simulation of lattice defects, P. C. Gehlen, J. R. Beeler, R. I. Jaffee Eds. (Plenum, New York, London, 1972) p. 217.
[19] Hoover H. G., Ladd A. J. C., Moran B., *Phys. Rev. Lett.* **48** (1982) 1818.
[20] Finney J. L., *Proc. R. Soc. London Ser. A* **319** (1970) 479.
[21] Gellatly B. J., Finney J. I., *J. Non-Cryst. Solids* **50** (1982) 313.
[22] Bellissent-Funel M. C., Roth M., Desré P., *J. Phys. F : Met. Phys.* **9** (1979) 987.
[23] Bradley A. J., Taylor A., *Philos. Mag.* **23** (1937) 1049.
[24] Srolovitz P., Maeda K., Takeuchi S., Egami T., Vitek V., *J. Phys. F : Met. Phys.* **11** (1991) 2209.
[25] McGreevy R. L., Pusztai L., *Mol. Simul.* **1** (1988) 459.